ELSEVIER

Biochimica et Biophysica Acta 1191 (1994) 65–78

BBA Biochimica et Biophysica Acta

Re-examination of hexose exchanges using rat erythrocytes: evidence inconsistent with a one-site sequential exchange model, but consistent with a two-site simultaneous exchange model

R.J. Naftalin *, R.J. Rist

Physiology Group, Biomedical Sciences Division, King's College London, The Strand, London WC2R 2LS, UK

(Received 14 October 1993)

Abstract

(1). The kinetic parameters of *zero-trans* net uptake and *infinite-trans* uptake of 3-*O*-methyl-D-glucoside, 2-deoxy-D-glucose and D-mannose into rat red cells at 24°C were measured after taking account of the linear diffusion components of flux. (2). *Zero-trans* exits of 3-*O*-methyl-D-glucoside and D-mannose from rat cells were also measured. (3). After correction for linear flux via non-specific routes, the V_{max} of *zero-trans* uptake of 3-*O*-methyl-D-glucoside was significantly higher, (1.25 ± 0.06 μmol(10 min)$^{-1}$(ml cell water)$^{-1}$) than the corresponding parameters of mannose or 2-deoxy-D-glucose, (0.33 ± 0.01 and 0.39 ± 0.01 μmol(10 min)$^{-1}$(ml cell water)$^{-1}$, respectively; $P < 0.001$). (4). After correction for linear flux via non-specific uptake routes, the V_{max} of *zero-trans* exit of 3-*O*-methyl-D-glucoside is significantly higher (1.70 ± 0.1 μmol(10 min)$^{-1}$(ml cell water)$^{-1}$) than the corresponding value for mannose exit flux, (1.10 ± 0.1 μmol(10 min)$^{-1}$(ml cell water)$^{-1}$; $P < 0.001$). (5). The acceleration ratio, i.e., the ratio of *infinite-trans* influx V_{max}/*zero-trans* influx V_{max} of mannose by mannose (9.12 ± 0.03) is significantly higher than that of 3-*O*-methyl-D-glucose by 3-*O*-methyl-D-glucose (2.77 ± 0.14)($P < 0.001$). (6). The one-site simple carrier model of glucose transport in which sugar exchange is viewed as a sequential process, predicts that the acceleration ratio of the more rapidly moving sugar 3-*O*-methyl-D-glucose by 3-*O*-methyl-D-glucose should be greater than that of the slower sugar, mannose by mannose. Hence, the observed findings are inconsistent with the one-site model, but confirm the earlier disputed studies of Miller, D.M. (1968; Biophys. J. 8, 1329–1338). (7). A two-site model, in which sugar exchange is considered as a simultaneous process, predicts that the acceleration ratio of mannose influx by mannose should be higher than for 3-*O*-methyl-D-glucose by 3-*O*-methyl-D-glucose. The data are, therefore, consistent with a two-site model.

Key words: Exchange transport kinetics; Red cell; Mannose; 3-*O*-Methyl-D-glucose; 2-Deoxy-D-glucose; (Rat)

1. Introduction

Numerous attempts have been made during the last quarter century to explain the mechanism of glucose transport across red cell membranes via the specific transporter protein, now identified as the Glut 1 transporter [1–5]. Four kinds of argument have been advanced, either in support or as a rejection of the 'simple carrier' hypothesis.

(i) Kinetic rejection criteria. Various combinations of the measured kinetic parameters (K_m and V_{max}) for inward and outward net flux and exchange flux taking the form of algebraic identities are used to determine whether the transport process is consistent with a one-site 'simple transporter'. The basis for these identities derives from the 'Haldane relationships', i.e., $V_{max,in}/K_{m,in} = V_{max,out}/K_{m,out}$ and the Principle of Microscopic Reversibility, which requires that at equilibrium the products of all the forward and backward rates in a cyclic reaction involving the several intermediate states are equal; i.e., $k_1 \cdot k_2 \cdot k_3 = k_{-1} \cdot k_{-2} \cdot k_{-3}$.

Early work showed that the observed parameters of glucose transport were inconsistent with the simple

* Corresponding author. Fax: +44 71 8732286.

0005-2736/94/$07.00
SSDI 0005-2736(93)E0381-J

carrier [6-8]. However, recently, revised parameters obtained from more rapid sampling techniques, are more consistent with the simple carrier [9-11].

A number of complexities, external to the transporter itself, interfere with interpretation of sugar fluxes; series barriers to sugar equilibration within the cytosol, i.e., non-specific binding of sugar to haemoglobin [2,12-14], create a diffusion barrier within the cytosol and reduce the accuracy of determinations of intracellular sugar concentration. The diffusion barrier raises the apparent K_m for *zero-trans* exit and reduces both the apparent K_m and apparent V_{max} for *zero-trans* net uptake [2,15]. Assessments of flux parameters based on integrated rate equations are particularly prone to this kind of inaccuracy and therefore differ from parameters derived from initial rates [13,15].

In cells with slow rates of transport, e.g., rat red cells, *parallel flows* via non-specific leak pathways are another potential source of error in estimating the membrane flux parameters [15,16].

Additionally, as with discontinuously collected sugar transport data, quite large deviations from ideal hyperbolic Michaelis-Menten kinetics are not readily detectable: it is evident that no unambiguous discrimination between one- or two-site models can be made on the basis of kinetic rejection criteria applied to the human red cell sugar transport system.

(ii) Inhibitor studies. A second approach to determining whether the sugar transporter has one or two sugar binding sites is to observe the effects of binding of non-transported inhibitor ligands on transport and ligand binding. Cytochalasin B binds preferentially to the inward facing site, whereas phloretin binds to the outward facing site. Hence, if there are two ligand binding sites on the transporter, both cytochalasin B and phloretin should bind without interference; whereas, once either ligand binds to a single site transporter it will prevent binding of the alternate ligand to the same carrier. Mutual interference between the binding of cytochalasin B and phloretin has been demonstrated, suggesting a single site [17-19]. However, it has also been found that prior binding of either ligand to the transporter merely reduces the affinity of the alternate ligand [20]. Thus, whether the paucity of doubly liganded transporter forms is a consequence of ligand binding to a one-site transporter, or to allosteric inhibition of ligand binding to a two-site transporter is indeterminate.

Non-transported sugars, with a high affinity for the transporter, e.g., the disaccharide maltose, when present in the bathing solution, act as unilateral inhibitors and are deemed to fix the carrier in an outward facing direction, thereby reducing cytochalasin B binding to the inward facing carrier site. As cytochalasin B binding is reduced by maltose, the experimental results favour one-site kinetics [21]. However, here too interpretation is compromised by the possibility of allosteric inhibition of cytochalasin B binding [20].

(iii) Pre-steady state kinetics. A third means of discriminating between one- and two-site sugar transport kinetics has been to observe 'pre-steady state' kinetics, with rapid detection of radioisotope uptake into red cells following a temperature jump, or rapid replacement of maltose in the external bathing solution by glucose [10,22]. High resolution, spectrofluorometric and spectrophotometric methods have also been used to observe the time-course of sugar-induced and cytochalasin B-inhibitable conformation changes, indicated by changes in quench of the intrinsic fluorescence of the amino-acid side chains within the sugar transporter. Following changes in external glucose concentration, the resulting conformational change, at least partially, reflects the movement of liganded carrier. However, these changes could stem from ligand penetration through the transporter to the second site; so the relationship of the relaxation processes to carrier movement across the membrane remains unclear [23-25].

Thus, although the weight of opinion supports the one-site model, there is insufficient evidence to reject either the one- or two-site transport models outright. This unsatisfactory situation arises because none of the tests so far described seek to discriminate between the different modes of exchange envisaged by the one- and two-site models.

(iv) Testing for differences in exchange modes.

(a) One-site predictions. The assumptions of the one-site circulating carrier model differ in two fundamental ways from the two-site model. Firstly, net flux is assumed to occur by *cis-trans* movement of loaded carrier and the sequential return of the empty carrier from *trans-cis* is required to complete the cycle. The rates of movement of loaded (k_3 or k_4) and unloaded carrier (k_2) (Diagram 1) are independently variable. Thus, when the transporter is unilaterally exposed to a high concentration of sugar, there may be a shift in the distribution of liganded and unliganded forms between the two surfaces.

The second assumption is that exchange results from *cis-trans* movement of loaded carrier, followed by a sequential return of carrier loaded with sugar abstracted from the *trans* pool of sugars. Since the exchange cycles consist only of partial reactions shared with the net flux cycles, it follows that the exchange cycles are fully delimited by constants which define the net flux cycles. This constraint, also applies to exchanges between different sugars (hetero-exchanges) with differing rates of transport and affinities.

Since the rate of unliganded carrier movement, k_2 is independent of the rate at which the liganded carrier moves, i.e., is invariant for all sugars, it follows that the sugar with the fastest *zero-trans* V_{max} $\{f(k_2 \cdot k_3)\}$ should also have the fastest *exchange* V_{max} $\{f(k_3 \cdot k_3)\}$ and the ratio of *infinite-trans* V_{max} to *zero-trans* V_{max} of this sugar $\{f(k_3/k_2)\}$ should also be the largest.

(b) Two-site predictions. The two-site transporter model implies firstly, that only the transported solutes, but not the binding sites, move between *cis* and *trans* sides; although conformation changes may occur during ligand translation, the *cis* sites remain accessible to ligands from the *cis* bathing solution during the entire transport process. Secondly, the simultaneous exchange of sugars between the alternate sites implies that the partial reactions for exchange and net flux differ.

The two-site model predicts that the resistance to flow of a slowly moving sugar across the membrane is larger than for a more rapidly moving sugar, i.e., *zero-trans* $V_{max} = f(k_3)$ (Diagram 2). The increase in ligand mobility $f(k_{ex})$ during exchange could arise from a fluidity increase within the transporter in the proximity of the bound ligands. Acceleration of exchange flux over net flux could arise because binding of the second ligand at the *trans* site reduces the *cis-trans* resistance to flow of the first ligand to some minimal level. Consequently, a slow sugar with a higher resistance to net flow across the transporter would be accelerated by switching to the exchange mode to a greater extent than would a fast sugar. These contrasting predictions of the one- and two-site mechanisms can be used as rejection criteria of either model.

Early studies with human red cells at 20°C in which *zero-trans*, or *equilibrium exchange* exits of radiolabelled glucose, galactose or mannose were observed, showed that galactose and mannose equilibrate more rapidly than glucose [26,27]. Contrary to the predictions of the one-site simple carrier, the ratio of glucose exchange flux to net glucose flux was larger than the ratio of mannose exchange to mannose net flux. However, it was suggested that this result could arise because glucose has a higher affinity for the transporter than either galactose, or mannose; hence, auto inhibition of labelled glucose uptake would be greater than with either galactose or mannose [26]. Because of the very high rates of sugar equilibration across human red cell membranes, these arguments had considerable force.

Rat erythrocyte membranes, have only 0.1% of the amount of glucose transporter that human red cell membranes have; consequently rat cells have a much lower rate of sugar transport than human cells, i.e., any change in sugar content of human red cells in 1 s requires approx. 10 min to effect an equivalent change in rat red cells [15]. This means that initial rates of net and exchange sugar transport can be examined with much higher precision in rat red cells than human cells. Accordingly, we have examined all the possible exchanges of 3-*O*-methyl D-glucopyranoside, D-mannose and 2-deoxy-D-glucose in rat red cells to test the predictions of the one-site and two-site models for exchange.

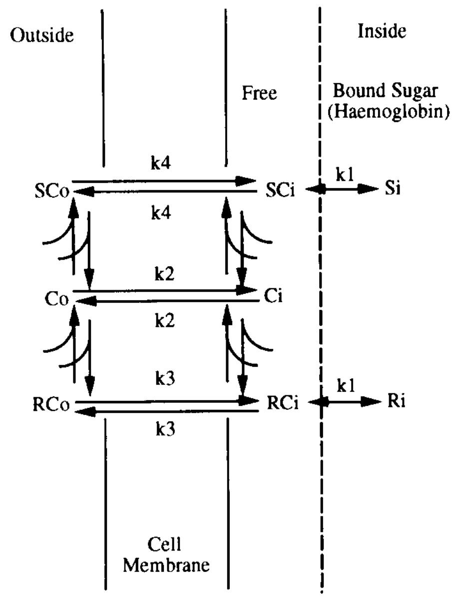

Diagram 1. Diagrammatic representation of the one-site sequential exchange model of sugar transport across the cell membrane in rat erythrocytes. C_o = carrier outside; C_i = carrier inside; k_2 = the symmetrical rate constant of free carrier movement; k_3 = the symmetrical rate constant of carrier liganded to sugar, R; k_4 = the symmetrical rate constant of carrier liganded to sugar, S.

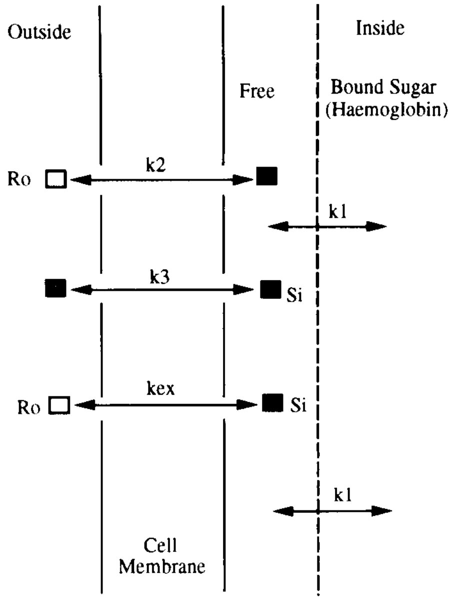

Diagram 2. Diagrammatic representation of the two-site simultaneous exchange model of sugar transport across the cell membrane in rat erythrocytes. k_2 = the symmetrical rate constant of carrier liganded to sugar, R; k_3 = the symmetrical rate constant of carrier liganded to sugar, S; k_{ex} = the symmetrical rate constant of exchanging carrier.

2. Materials and methods

Cells. Erythrocytes were obtained by exsanguination of 100–200 g Wistar rats, which had been anaesthetised with diethyl ether and killed by cervical dislocation. The cells were washed twice in isotonic NaCl-Hepes buffer (pH 7.3) by repeated centrifugation at room temperature at $4000 \times g$ to remove plasma, white cells and intracellular sugar.

Hepes buffer. The Hepes buffer contained 140 mM NaCl, 5 mM KCl, 1.2 mM $MgCl_2$, 5 mM Hepes (*N*-2-hydroxyethylpiperazine-*N*-2-ethanesulfonic acid; sodium salt) (Sigma) at pH 7.3.

Stopping solution. Stopping solution consisted of NaCl-Hepes buffer at 2–4°C containing phloretin and $HgCl_2$ at final concentrations of 100 μM and 1 μM, respectively. Additionally, cytochalasin B (5 μM) was added to the stopping solution during the measurement of non-specific linear uptakes of sugar.

Cell numbers and cell volume. Cell numbers were estimated using a Coulter Counter model B and also an Elzone 280 PC cell counter. The intracellular concentration of sugar was estimated on the basis that $3 \cdot 10^{10}$ cells $\equiv$ 1 ml cell water. No correction was applied for the small changes in intracellular volume caused by the small initial difference in intracellular and extracellular tonicity due to asymmetric loading concentrations of sugar.

Radioisotopes. All the radioactive sugars were obtained from Amersham International (UK). The sugars used were D-[2-^{3}H]mannose, 2-deoxy-D-[2,6-^{3}H]glucose and 3-*O*-methyl-D-[1-^{3}H]glucose and the final activity for all sugars used was between 0.5 and 1 μCi/ml for both influx and efflux experiments.

Zero-trans net entry. Freshly isolated rat red blood cells were pre-incubated for 4 h at 37°C in sugar-free saline, in order to reduce the concentration of endogenous internal sugar. The erythrocytes were then washed in ice-cold buffer and 200 μl of this suspension was added to 3 ml of isotonic Hepes buffer in test tubes containing varying concentrations (1–40 mM) of ^{3}H-labelled sugar (Amersham). Uptake of sugar was then measured over 10 min at 24°C in a shaking water bath. During this time the concentration of sugar within the cells rose to approx. 5% of the external solution, assuming a single intracellular compartment. The uptake was stopped by addition of ice-cold stopping solution to the test tubes, which were then placed on ice and the cells were pelleted by centrifugation at $4000 \times g$ for 2 min. Following two further washes, the radioactivity was extracted from the dispersed cell pellets by addition of 1.5 ml 5% trichloroacetic acid. The radioactivity of aliquots of the deproteinized extracts and extracellular fluid were counted using scintillation fluid containing 500 ml toluene, 500 ml Synperonic NX (Durham Chemical Distributors, Birtley, Chester-le-Street, Durham, UK), and 2.5 g of 2.5-diphenyloxazole (Sigma, Poole, Dorset, UK).

Infinite-trans exchange uptake. Erythrocytes were preloaded with 50 mM unlabelled sugar at 37°C for 4 h, washed in ice-cold, sugar-free buffer and then the uptake of varying concentrations (1–40 mM) of ^{3}H-labelled sugar (Amersham) was measured over 10 min at 24°C, as described for *zero-trans* uptake. The uptake was stopped with ice-cold stopping solution and the radioactivity of the samples determined as before.

Zero-trans net exit. Following an initial pre-loading period of 2–4 h at 37°C with varying concentrations (1–40 mM) of ^{3}H-labelled sugar at a haematocrit of 30%, the cells were pelleted and 0.5 ml of packed cells, (85% haematocrit) was added to 50 ml of Hepes buffer at 24°C or ice-cold stopping solution containing cytochalasin B (5 μM). The cells were dispersed and at intervals over a 60 min time-course, 1.5-ml aliquots of the cell suspension were added to ice-cold stopping solution and centrifuged. The cell pellets were extracted in 5% trichloroacetic acid as described above and the radioactivity counted.

Infinite-trans exchange exit. Erythrocytes pre-loaded for 2–4 h at 37°C with 40 mM ^{3}H-labelled sugar were pelleted and then 0.5 ml of packed cells was added to 50 ml of Hepes buffer containing 20 mM unlabelled sugar. The exit of the labelled sugar was then followed over a 60 min period as described for *zero-trans net exit* and the radioactivity of the samples measured as before.

Three-parameter fits. In order to estimate the Michaelis-Menten parameters of the sugar influxes and effluxes, the linear non-specific leak components were determined. The data were fitted to three-parameter plots as follows:

$$v = V_{max} \cdot S/(K_m + S) + k_l \cdot S$$

where V_{max} and K_m are the Michaelis-Menten parameters; k_l is the linear leakage coefficient and S is the sugar concentration (mM) in the *cis* bathing solution. All three parameters together with their standard errors are estimated by non-linear least-squares regression, using the fitting program of Kaleidagraph 2.1 (Abelbeck Software). The linear leakage rate was also estimated directly from the rates of sugar uptake and exit in the presence of stopping solution containing cytochalasin B (5 μM).

Statistics. All data are expressed as means $\pm$ S.E.; the numbers of data points used are as stated in the text. The S.E. of derived parameters are obtained from the least-squares regression lines. The significance levels of any differences are determined from Student's *t*-test using appropriate degrees of freedom and the errors of ratios are obtained by Gaussian summation.

Models of one-site and two-site sugar transport kinetics with internal linear binding compartment. The one-

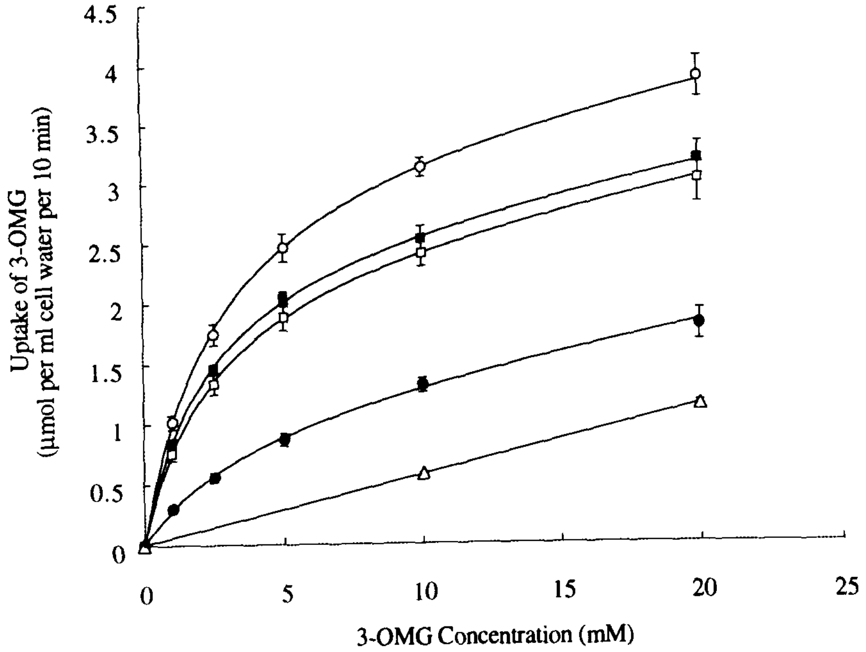

Fig. 1. Effects of pre-loading with 3-OMG, mannose and 2-dGlc on the uptake of 3-OMG by rat erythrocytes. Freshly isolated rat red blood cells were preloaded with (*infinite-trans*) or without (*zero-trans*) 50 mM 3-OMG, mannose or 2-dGlc for 4 h at 37°C. The cells were then washed free of external sugar and the uptake of varying concentrations of 3-OMG (1–40 mM) were measured over 10 min at 24°C in Hepes buffer or stopping solution containing cytochalasin B (5 μM). The data shown are means ± S.E. ($n = 8$) and lines are fitted by non-linear least-squares regression using a Kaleidagraph 2.1 (Abelbeck Software) three-parameter fit, (except cytochalasin B data, which is a one-parameter fit). *Zero-trans* uptake, closed circles; *infinite-trans* uptake with 3-OMG, open circles; *infinite-trans* uptake with mannose, closed squares; *infinite-trans* uptake with 2-dGlc, open squares; *zero-trans* uptake with stopping solution and cytochalasin B (5 μM), open triangles.

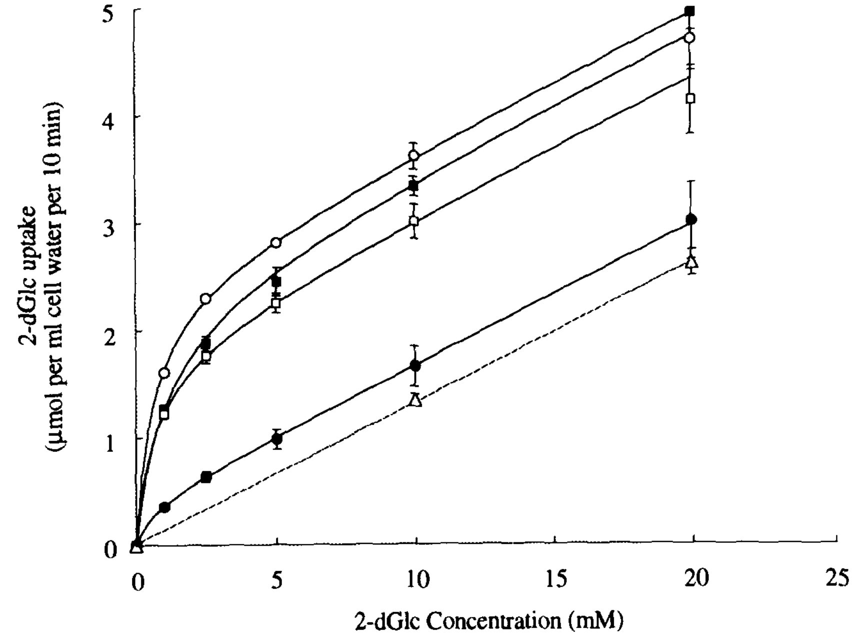

Fig. 2. Effects of pre-loading with 3-OMG, mannose and 2-dGlc on the uptake of 2-dGlc by rat erythrocytes. Freshly isolated rat erythrocytes were preloaded with (*infinite-trans*) or without (*zero-trans*) 50 mM 3-OMG, mannose or 2-dGlc for 4 h at 37°C. The cells were then washed with ice-cold saline to remove external sugar and the uptake of varying concentrations of radiolabelled 2-dGlc (1–40 mM) were measured over 10 min at 24°C in Hepes buffer or stopping solution containing cytochalasin B (5 μM). The data shown are means ± S.E. ($n = 8$) and the Michaelis-Menten parameters were calculated with a three-parameter fit using Kaleidagraph 2.1 (Abelbeck Software). *Zero-trans* uptake, closed circles; *infinite-trans* uptake with 3-OMG, open circles; *infinite-trans* uptake with mannose, closed squares; *infinite-trans* uptake with 2-dGlc, open squares; *zero-trans* uptake with stopping solution and cytochalasin B (5 μM), open triangles.

site and two-site models were simulated with the aid of Stella II.2.2.1 (High Performance Systems) a modelling package for the Macintosh computer which facilitates model construction and solution of the time-differential equations used to simulate transport networks. The equations are solved numerically with fourth-order Runge Kutta integration procedures and are shown in the Appendices 1 and 2.

Sugar uptake into and exit from the cells is simulated to mimic the experimental conditions used in this paper. As previously described [14] the modelled cells have a compartment of haemoglobin occupying 85% of the cell volume into which glucose equilibrates slowly from the free compartment. This compartment is identical in both one-site and two-site simulations.

3. Results

Zero-trans uptake of 3-O-methyl-D-glucoside (3-OMG), 2-deoxy-D-glucose (2-dGlc) and D-mannose

Zero-trans net uptake of varying concentrations (1–40 mM) of 3-OMG, 2-dGlc and mannose were measured over 10 min at 24°C, (Figs. 1, 2 and 3). Initial experiments were undertaken to ensure that the time-course of uptake was linear during the period of measurement for each of the sugars and it was found that replicated uptake measurements over 10 min give accurate estimates of influx. To calculate the Michaelis-Menten parameters, the linear non-specific leak component of flux was determined from uptake of sugar in the presence of stopping solution containing cytochalasin B (5 μM) and this was then subtracted from the raw data. All data points shown are obtained from four separate experiments which consisted of two replicates each, i.e., $n = 8$.

Infinite-trans uptakes of 3-OMG, 2-dGlc and mannose

Erythrocytes were pre-loaded with 50 mM unlabelled 3-OMG, 2-dGlc, or mannose for 4 h at 37°C and then the *infinite-trans* uptake of varying concentrations (1–40 mM) of radiolabelled 3-OMG, 2-dGlc and mannose was measured over 10 min at 24°C, (Figs. 1, 2 and 3). Initial experiments in which the loading concentrations of all the sugars was varied from 20 to 60 mM were undertaken to examine the linearity of flux and the loading concentration which would give maximal acceleration. Maximal acceleration was attained at loading concentrations > 20 mM and uptake of isotope was linear over the 10 min period.

The *zero-trans* net uptake of the 3-OMG, 2-dGlc and mannose were also estimated in the presence of stopping solution with cytochalasin B (5 μM) (Figs. 1, 2 and 3). The best-fit linear regression lines were fitted to these uptakes in order to determine the rate of non-specific leakage of 3-OMG, 2-dGlc and mannose.

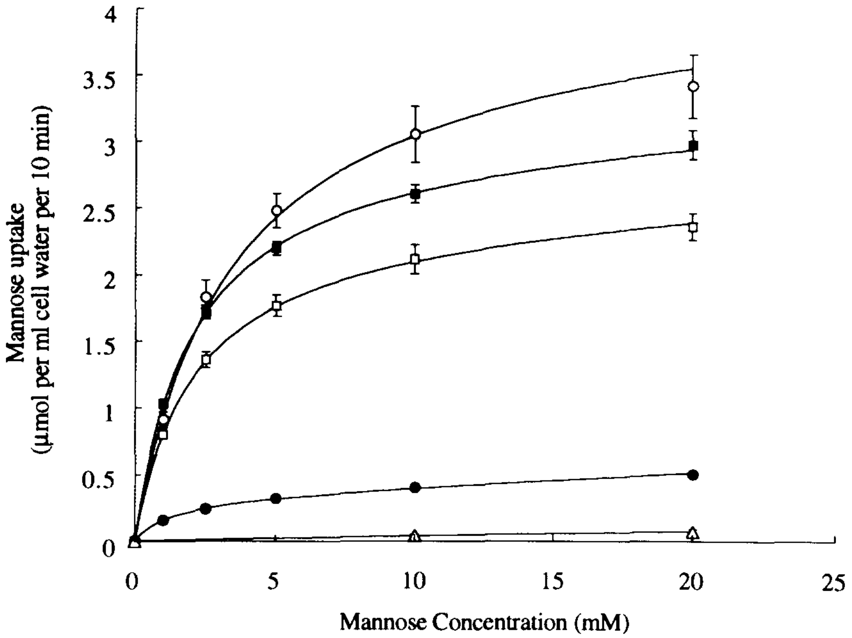

Fig. 3. Effects of pre-loading with 3-OMG, mannose and 2-dGlc on the uptake of mannose by rat erythrocytes. Rat red blood cells were preloaded with (*infinite-trans*) or without (*zero-trans*) 50 mM 3-OMG, mannose or 2-dGlc for 4 h at 37°C. The cells were then washed free of external sugar and the uptake of varying concentrations of mannose (1–40 mM) were measured over 10 min at 24°C in Hepes buffer or stopping solution containing cytochalasin B (5 μM). The data shown are means ± S.E. ($n = 8$) and the Michaelis-Menten parameters were estimated by non-linear least-squares regression using Kaleidagraph 2.1 (Abelbeck Software). *Zero-trans* uptake, closed circles; *infinite-trans* uptake with 3-OMG, open circles; *infinite-trans* uptake with mannose, closed squares; *infinite-trans* uptake with 2-dGlc, open squares; *zero-trans* uptake with stopping solution and cytochalasin B (5 μM), open triangles.

Table 1
Transport parameters for *zero-trans* and *infinite-trans* uptake of mannose, 3-OMG and 2-dGlc by rat erythrocytes

Transported sugar	Transport mode	V_{max}	Acceleration ratio	K_m	Diffusion constant
Mannose	*Zero-trans*	0.33 ± 0.01	–	1.22 ± 0.11	0.010 ± 0.001
	Infinite-trans (3-OMG)	3.88 ± 0.14 [a]	11.76 ± 0.05	3.15 ± 0.24 [a]	0.010 ± 0.001
	Infinite-trans (mannose)	3.01 ± 0.02 [a,b]	9.12 ± 0.03 [b]	1.95 ± 0.03 [a]	0.010 ± 0.001
	Infinite-trans (2-dGlc)	2.41 ± 0.02 [a,b]	7.30 ± 0.03 [b]	2.03 ± 0.03 [a]	0.010 ± 0.001
3-OMG	*Zero-trans*	1.25 ± 0.06 [c]	–	4.11 ± 0.39 [c]	0.040 ± 0.002 [c]
	Infinite-trans (3-OMG)	3.46 ± 0.04 [a]	2.77 ± 0.14 [c]	2.61 ± 0.09 [a]	0.040 ± 0.002
	Infinite-trans (mannose)	2.65 ± 0.04 [a,b]	2.12 ± 0.11 [b]	2.28 ± 0.07 [a]	0.040 ± 0.002
	Infinite-trans (2-dGlc)	2.53 ± 0.02 [a,b]	2.02 ± 0.10 [b]	2.53 ± 0.05 [a]	0.040 ± 0.002
2-dGlc	*Zero-trans*	0.39 ± 0.01	–	0.70 ± 0.07 [c]	0.13 ± 0.01 [c]
	Infinite-trans (3-OMG)	2.43 ± 0.02 [a]	6.23 ± 0.16 [c]	0.62 ± 0.04	0.13 ± 0.01
	Infinite-trans (mannose)	2.25 ± 0.08 [a]	5.77 ± 0.25	0.99 ± 0.09	0.13 ± 0.01
	Infinite-trans (2-dGlc)	1.80 ± 0.03 [a,b]	4.62 ± 0.14 [b]	0.65 ± 0.04	0.13 ± 0.01

This table shows the Michaelis-Menten parameters for mannose, 3-OMG and 2-dGlc uptake calculated from the three parameter fits used in Figs. 1, 2, and 3. The acceleration ratio is calculated from the maximal rate of *infinite-trans* exchange uptake divided by the maximal rate of *zero-trans* uptake and the diffusion constant is the average of the non-specific leak component of uptake measured in the presence of stopping solution and cytochalasin B (5 μM) and the calculated leak from the three-parameter regression lines. V_{max} and diffusion constant values are expressed as μmol $(10\ \text{min})^{-1}$ (ml cell water)$^{-1}$ and K_m values are given as mM. [a] $P < 0.001$, for test versus *zero-trans* value for the same sugar; [b] $P < 0.001$, for test versus *infinite-trans* (3-OMG) value for the same sugar; [c] $P < 0.001$, for test versus equivalent value for mannose.

In addition, the data for the *infinite-trans* uptakes of 3-OMG, 2-dGlc and mannose were fitted using best-fit non-linear three-parameter regression lines and the linear leakage rates (diffusion constants) of the three sugars were estimated mathematically from these regression lines.

The estimated and the measured linear leakage rates of 2-dGlc exceed those of 3-OMG ($P < 0.001$) and those of 3-OMG exceed those of mannose, ($P <$ 0.001). The Michaelis-Menten parameters obtained for the three-parameter fits are shown in Table 1.

The V_{max} for *zero-trans* uptake of 3-OMG exceeds

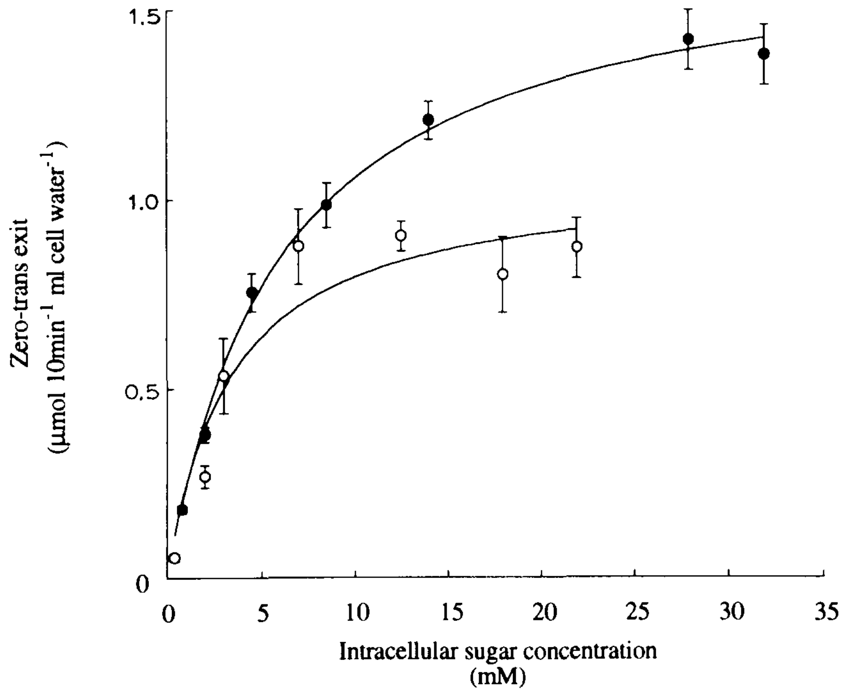

Fig. 4. *Zero-trans* exit of varying concentrations of 3-OMG and mannose from rat erythrocytes. Rat red blood cells were pre-loaded for 2–4 h at 37°C with varying concentrations (1–40 mM) of ^{3}H-labelled 3-OMG or mannose. The erythrocytes were then dispersed in sugar-free buffer at 24°C or ice-cold stopping solution containing cytochalasin B (5 μM) and the exit of the radiolabel followed over the subsequent 60 min. The data are means $\pm$ S.E. ($n = 8$) over the initial 10 min following transfer to sugar-free buffer and have been corrected for non-specific leakage of 3-OMG or mannose by subtracting the appropriate cytochalasin B-insensitive efflux. The Michaelis-Menten values are estimated from a two-parameter fit using Kaleidagraph 2.1, (Abelbeck Software) and are shown in Table 2. Mannose, open circles; 3-OMG, closed circles.

that of mannose ($P < 0.001$) and 2-dGlc by 3–4-fold, (Table 1). The K_m for *zero-trans* 3-OMG influx also exceeds that of mannose influx by 3–4-fold ($P < 0.001$).

The acceleration ratio of mannose by mannose (9.12 $\pm$ 0.03) exceeds that of 3-OMG by 3-OMG, (2.77 $\pm$ 0.14) ($P < 0.001$). Mannose is maximally accelerated by 3-OMG by 11.76 $\pm$ 0.05-fold and is accelerated by 2-dGlc to a lesser extent (7.3 $\pm$ 0.03-fold). 3-OMG, 2-dGlc and mannose are all accelerated most by *trans* 3-OMG and least by *trans* 2-dGlc ($P < 0.001$).

Zero-trans net exit

Erythrocytes were pre-loaded for 4 h at 37°C with varying concentrations (1–40 mM) of radiolabelled 3-OMG and mannose, before being washed and then dispersed in Hepes buffer at 24°C or ice-cold stopping solution containing cytochalasin B (5 μM). The rates of *zero-trans* net exit of the two sugars from the cells over the initial 10 min are shown in Fig. 4 and have been corrected for non-specific leakage by subtracting the stopping solution-insensitive efflux.

The intracellular concentrations of the two sugars displayed on the abscissa are the mean values measured immediately after transfer of the erythrocytes into sugar-free solutions. It is assumed that this sugar is distributed uniformly within the cells during the time of efflux. The error estimates of these intracellular concentrations (about $\pm$5% of mean values) are omitted. The data are fitted by non-linear regression to the two-parameter Michaelis-Menten equation and the best-fit parameters $\pm$S.E. are shown in Table 2.

A modest asymmetry is observed between mannose net entry and exit; the *zero-trans* V_{max} for entry is 0.33 $\pm$ 0.01 μmol(10 min)$^{-1}$(ml cell water)$^{-1}$, whereas the *zero-trans* V_{max} for exit is 1.1 $\pm$ 0.1 μmol(10 min)$^{-1}$(ml cell water)$^{-1}$ ($P < 0.001$); the K_m for *zero-trans* net mannose uptake is 1.22 $\pm$ 0.11 mM, whereas, the K_m for *zero-trans* net exit is 3.31 $\pm$ 1.39 mM.

The net fluxes of 3-OMG are more symmetrical than those of mannose. The *zero-trans* V_{max} for 3-OMG influx is 1.25 $\pm$ 0.06 μmol(10 min)$^{-1}$(ml cell water)$^{-1}$ and the *zero-trans* V_{max} for efflux is 1.7 $\pm$ 0.1. The K_m for *zero-trans* uptake of 3-OMG is 4.11 $\pm$ 0.39 mM, whereas the K_m for *zero-trans* exit is 6.02 $\pm$ 0.53 mM.

Infinite-trans exchange exit

The rates of exchange exit of labelled 3-OMG, or mannose from cells into 20 mM 3-OMG or mannose were also measured.

Previously, we were unable to demonstrate acceleration of 10 mM 3-OMG exit by 20 mM 3-OMG [14]. Here, however, there was a significant acceleration of *infinite-trans* exchange exit from cells loaded with 23 $\pm$ 4 mM 3-OMG by 20 mM 3-OMG (Table 2) ($P < 0.01$). These data confirm the findings of Helgerson and Carruthers [15].

However, the observed rates of exchange exit were less than the rates of exchange uptake, i.e., the maximal rate of exchange uptake of mannose into mannose is 3.01 $\pm$ 0.02 μmol(10 min)$^{-1}$(ml cell water)$^{-1}$; whereas exchange exit of mannose by mannose is 1.5 $\pm$ 0.1 μmol(10 min)$^{-1}$(ml cell water)$^{-1}$ ($P < 0.001$). The maximal rate of exchange uptake of 3-OMG into 3-OMG is 3.46 $\pm$ 0.04 μmol(10 min)$^{-1}$(ml cell water)$^{-1}$;, whereas the measured rate of exchange exit of 3-OMG by 3-OMG is 2.0 $\pm$ 0.2 μmol(10 min)$^{-1}$(ml cell water)$^{-1}$ ($P < 0.001$). This apparent asymmetry is due to slow sugar equilibration within the intracellular compartments and the relatively long time required to measure exit accurately (30–60 min) from cells loaded with high concentrations of sugar. It seems likely, therefore that the values shown in Table 2 are under-estimates of the rates of exchange exit.

4. Discussion

3-OMG has a higher mobility than mannose across rat red cell membranes

The maximal rates of 3-OMG net flux are faster than those of mannose. The *zero-trans* V_{max} for mannose net entry is 26% of that of 3-OMG ($P < 0.001$) (Table 1) and the *zero-trans* V_{max} of mannose net exit is 65% of that found for 3-OMG ($P < 0.001$)(Fig. 4). The K_m for *zero-trans* uptake of mannose is 1.22 $\pm$ 0.11 mM and the K_m for *zero-trans* exit is 3.31 $\pm$ 1.39 mM. 3-OMG has a significantly higher *zero-trans* entry K_m (4.11 $\pm$ 0.39 mM) than mannose ($P < 0.001$; Table 1),

Table 2
Transport parameters for *zero-trans* and *infinite-trans* exit of mannose and 3-OMG by rat erythrocytes

Intracellular sugar (mM)	*z–t* exit flux	*i–t* exit mannose	Acceleration ratio	*i–t* exit 3-OMG	Acceleration ratio
Mannose (17.2 $\pm$ 2.9 mM)	0.9 $\pm$ 0.1	1.5 $\pm$ 0.1 **	1.68 $\pm$ 0.10	1.4 $\pm$ 0.1 **	1.63 $\pm$ 0.08
3-OMG (23 $\pm$ 4 mM)	1.4 $\pm$ 0.1 **	2.1 $\pm$ 0.2 +,*	1.50 $\pm$ 0.12	2.0 $\pm$ 0.2 +,*	1.43 $\pm$ 0.08

Erythrocytes were pre-loaded with 40 mM ^{3}H-labelled mannose or 3-OMG for 2–4 h at 37°C and then dispersed in Hepes buffer at 24°C containing 20mM unlabelled mannose or 3-OMG. The exit of labelled sugar was measured over the following 60 min and the *zero-trans* and *infinite-trans* exits of the sugars are expressed as μmol (10 min)$^{-1}$ (ml cell water)$^{-1}$; means $\pm$ s.e., n = 8 and have been corrected for linear leak component. ** $P < 0.01$; * $P < 0.05$, for test versus *zero-trans* exit value for the same sugar; ++ $P < 0.01$; + $P < 0.05$, for test versus equivalent value for mannose.

although the K_m of 3-OMG exit (6.02 ± 0.53 mM) does not differ significantly from that of mannose. The higher affinity of mannose than 3-OMG for the external site suggests the possibility that mannose net influx may be subject to greater self-inhibition than that of 3-OMG and this could explain why 3-OMG has a higher observed *zero-trans* entry V_{max} than mannose.

However, simulation of sugar uptake, at the observed rates of net sugar uptake into a slowly equilibrating intracellular pool, over a range of inside site affinities of the transporter (K_d = 1–6 mM), indicates that self-inhibition due to a higher affinity of mannose for the internal site of the transport, would only reduce the V_{max} for *zero-trans* entry of mannose relative to the V_{max} of *zero-trans* 3-OMG entry by a maximum of 20%. Also, *zero-trans* efflux is not subject to self-inhibition; hence the observed difference between the *zero-trans* V_{max} of 3-OMG and mannose exit (V_{max} of 3-OMG exit is 1.55 ± 0.15-fold larger, than that of mannose, $P < 0.01$; Fig. 4). This confirms that the higher *zero-trans* influx V_{max} of 3-OMG is due to its higher mobility across the transporter and not because the affinity of mannose for the inside site of the transporter is higher than that of 3-OMG.

Because the errors of *zero-trans* and *infinite-trans* entry tend to cancel each other, the error in estimating the difference in acceleration ratio of mannose and 3-OMG entry (Table 1) due to greater self-inhibition of net mannose uptake, is < 10%.

Hence, the Results showing a higher acceleration ratio, i.e., *infinite-trans entry* V_{max}/*zero-trans entry* V_{max} of mannose than of 3-OMG (Table 1), can be attributed to a higher net flux mobility of 3-OMG than mannose within the membrane transport system and not to a lower affinity of 3-OMG than mannose for the transporter sites at the inside surface.

The relatively small acceleration ratios of *infinite-trans exit / zero-trans exit* in comparison with the acceleration ratios for uptake (Tables 1 and 2) are consistent with to a modest intrinsic asymmetry of net flux across the rat red cell system, but are also consistent with a series barrier to isotope equilibration within the cytosol. The small differences between exchange exit and net exit and the relative inaccuracy of the estimates of V_{max} of exchange exit reduce the value of these exit data for testing rival theories of exchange transport, so these data have been excluded from further consideration here.

Analysis of the results in terms of one- and two-site transport mechanisms

One-site sequential transporter. The basis of the acceleration of exchange as predicted by the one-site model is (a) that the liganded form of the carrier crosses the membrane faster than the unliganded free carrier and (b) accelerated exchange depends on return of liganded carrier loaded with sugar abstracted from the *trans* pool.

We have modelled the effects of varying k_2, the symmetrical rate constant of free carrier movement and k_3, the symmetrical rate constant of liganded carrier (Diagram 1) on the ratio of free carrier facing the inner surface c_i, to free carrier facing outward c_o, in the *zero-trans* condition. The conditions simulated have 20 mM sugar in the external solution and initially, zero internal sugar; the K_d values of the sugar at both inner and outer surfaces = 1 mM. The rate constants k_2 and k_3 were varied to include the observed range of mannose, 2-dGlc and 3-OMG net uptakes into rat cells at 24°C over 10 min (see Figs. 1, 2 and 3). As expected, from one-site model predictions, (see Introduction) the ratio c_i/c_o increases both as k_3 increases and as k_2 decreases. When $k_2 < 0.4$ and $k_3 > 2$ the ratio of c_i/c_o exceeds 100 and when $k_2 \approx k_3$ then $c_i/c_o \approx 1$.

The high ratios of c_i/c_o seen in the *zero-trans* condition, revert to values < 1 when the cells are loaded with 50 mM sugar, to simulate the *infinite-trans* exchange uptake condition. In the *infinite-trans* exchange mode, the rate of free carrier movement, k_2 has a negligible effect on the distribution ratio of free carrier. The dominant factors affecting the ratio in the *infinite-trans* condition are the rates of movement of liganded carrier, k_3 and k_4.

The effect of changing the model parameters k_2 and k_3 on simulated net sugar uptake during the initial 10 min of *zero-trans* entry is also shown as a contoured surface plot (Fig. 5). The predicted V_{max} for sugar uptake is an increasing function of both k_2 and k_3.

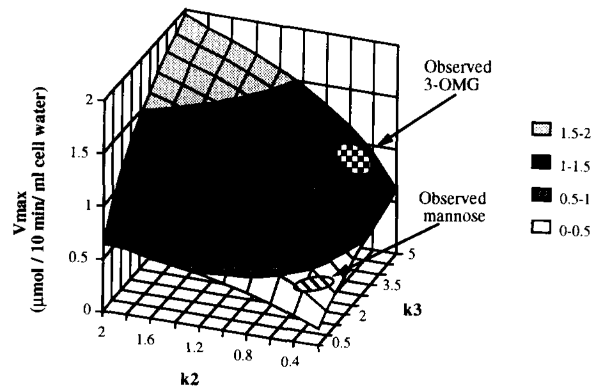

Fig. 5. Contoured surface plot from the one-site model simulating the effects of varying the rate constants k_2 and k_3 on the maximal rate of *zero-trans* uptake of sugar by rat red cells. This plot was obtained from data modelled using the Stella II.2.2.1 (High Performance Systems) package for the Macintosh computer. The 3-D plot was obtained using Microsoft Excel 4.0 and annotated using the drawing package, SuperPaint 2.0. This plot simulates the initial uptake (10 min) of 3-OMG and mannose by erythrocytes. The observed maximal rates of uptake (V_{max}) of mannose (striped ellipse) and 3-OMG (chequered ellipse) are also shown. k_2 = the symmetrical rate constant of free carrier movement; k_3 = the symmetrical rate constant of carrier; units = min^{-1}.

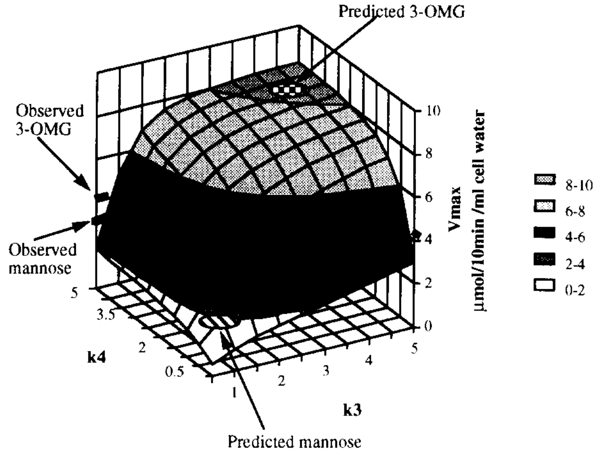

Fig. 6. Contoured surface plot from the one-site model simulating the effects of varying the rate constants k_3 and k_4 on the maximal rate of *infinite-trans* uptake of sugar by rat red cells. This plot shows a simulation of the maximal rate of *infinite-trans* exchange uptake of 3-OMG and mannose over 10 min by rat erythrocytes. The predicted maximal rates (V_{max}) of *infinite-trans* exchange uptake of mannose (striped ellipse) and 3-OMG (chequered ellipse) are superimposed on the surface of the plot and the observed maximal rates are marked on the vertical axis. k_3 = the symmetrical rate constant of sugar, R; k_4 = the symmetrical rate constant of sugar, S; k_2 is fixed at 0.4 min^{-1}.

This is consistent with the model requirement that the net flux cycle is a function of the product of $k_2 \cdot k_3$.

Zero-trans net sugar uptake in the range ≈ 0.3 μmol(10 min)$^{-1}$(ml cell water)$^{-1}$, equivalent to mannose uptake (Table 1) is shown as a striped ellipse; encompassing a range of k_2 from 0.25 to 0.45 min^{-1} and a range of k_3 from 0.8 to 1 min^{-1}. *Zero-trans* net sugar uptake ≈ 1.2 μmol(10 min)$^{-1}$(ml cell water)$^{-1}$, equivalent to 3-OMG uptake is shown as a chequered ellipse encompassing a range of k_2 from 0.3 to 0.5 min^{-1} and of k_3 from 3.75 to 4.25 min^{-1}.

By adopting the constraint that the free carrier mobility is independent of either sugar and is therefore the same for both sugars, the only appropriate values of the one-site parameters defining both mannose and 3-OMG uptake into rat red cells at 24°C are in the region of overlap, where k_2, the unoccupied carrier mobility, accommodates both sugar uptakes, i.e., $k_2 \approx$ 0.4 min^{-1}. For mannose $k_2 = 0.4$ min^{-1} and $k_3 \approx 1.0$ min^{-1} and for 3-OMG, $k_3 \approx 4.0$ min^{-1}.

The predicted maximal rates of sugar uptake in the *infinite-trans* condition are shown in Fig. 6. The rate of free carrier movement, k_2 is maintained at 0.4 min^{-1}, whilst the rates of liganded carrier movement, k_3 and k_4 are varied from 0.5 to 5.0 min^{-1}. The maximal rate of *infinite-trans* exchange influx is an increasing function of both k_3 and k_4, where k_4 is the rate of return of carrier complexed with sugar from the cytosol. This is consistent with the model prediction that the exchange flux cycle is a function of the product of k_3 and k_4. However, the observed exchange rate flattens when $k_3 > 2.0$ min^{-1} and the rate of exchange uptake exceeds 6 μmol(10 min)$^{-1}$(ml cell water)$^{-1}$. This is due to rapid accumulation of 'labelled' sugar from the external bath in the cytosolic free sugar compartment, with consequent high rates of labelled sugar reflux via the exchange transporter.

The predicted rate of *infinite-trans* mannose uptake into mannose ($k_2 = 0.4$ min^{-1}, $k_3 = k_4 = 1$ min^{-1} is shown within the area of the striped ellipse ≈ 1.8 μmol(10 min)$^{-1}$(ml cell water)$^{-1}$. The observed V_{max} $= 3.01 \pm 0.02$ μmol(10 min)$^{-1}$(ml cell water)$^{-1}$ (Table 1), i.e., the model prediction is 60% lower than the observed rate. The predicted *infinite-trans* V_{max} for 3-OMG entry into 3-OMG ≈ 8.5 μmol(10 min)$^{-1}$(ml cell water)$^{-1}$ ($k_2 = 0.4$ min^{-1}; $k_3 = k_4 = 4$–4.5 min^{-1}) is shown as a chequered ellipse superimposed on the surface plot, whilst the observed *infinite-trans* V_{max} of 3-OMG entry is 3.46 ± 0.04 μmol(10 min)$^{-1}$(ml cell water)$^{-1}$ (Table 1). Thus, the predicted rate of *infinite-trans* 3-OMG uptake into 3-OMG, on the basis of one-site kinetic parameters is 140% higher than the observed rate. It should be noted that the high predicted rate of 3-OMG rate would even higher were it not masked by the high rate of sugar recycling from the unstirred layer within the cytosol.

A contoured surface plot of the simulated acceleration ratio (entry), i.e., *infinite-trans entry* V_{max}/ *zero-trans entry* V_{max} is displayed in Fig. 7. The initial conditions are as for Fig. 6 and k_2 is held constant at

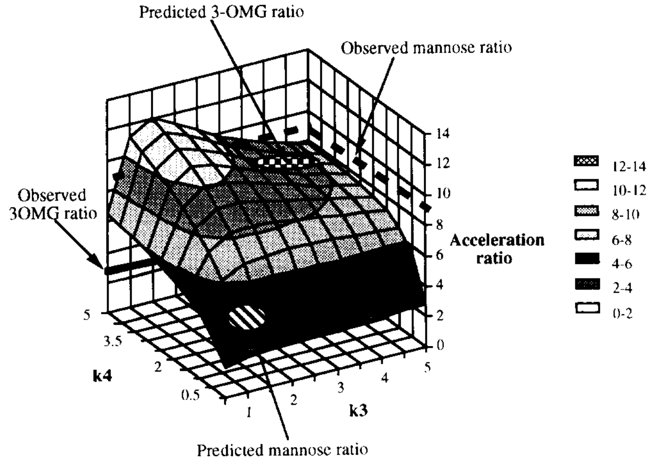

Fig. 7. Contoured surface plot from the one-site model simulating the effects of varying the rate constants k_3 and k_4 on the acceleration ratio of mannose and 3-OMG uptake in rat red cells. The acceleration ratio for sugar uptake is the maximal rate of *infinite-trans* exchange uptake divided by the maximal rate of *zero-trans* uptake. The predicted acceleration ratios for mannose (striped ellipse) and 3-OMG (chequered ellipse) are superimposed on the surface of the plot and the observed acceleration ratios for mannose (dotted line) and 3-OMG (solid line) are shown on the vertical axis. k_3 = the symmetrical rate constant of sugar, R; k_4 = the symmetrical rate constant of sugar, S; k_2 is fixed at 0.4 min^{-1}.

0.4 min^{-1}. The surface function of accelerated exchange is more complex than those shown in Figs. 5 and 6. The acceleration ratio is an increasing function of k_4 and also of k_3 in the range 0–1.5 min^{-1} as predicted (see Introduction), however, the acceleration ratio falls when k_3 increases above 2.0 min^{-1}. This secondary decrease, results from of incomplete equilibration of the newly absorbed sugar with the cytosol and its consequent higher rate of reflux (see above). It should be noted that this predicted reflux only occurs at sugar exchange rates which are about twice the observed maximal exchange rates (Table 1). In the observed range of sugar exchange uptakes, reflux does limit sugar uptake to a significant extent.

The predicted acceleration ratio of mannose by mannose is ≈ 4 (striped ellipse); whereas the observed acceleration ratio is 9.12 ± 0.03 (Table 1), i.e., the predicted acceleration ratio is only 43% of the observed value. The predicted acceleration ratio of 3-OMG by 3-OMG ≈ 8 (chequered ellipse), whereas the observed acceleration ratio of 3-OMG by 3-OMG is 2.77 ± 0.14 (Table 1); i.e., the predicted acceleration ratio of 3-OMG exceeds the observed ratio by 190%, (N.B. this takes account of unstirred layer effects which reduce the predicted uptake). Hence, the predictions of the one-site model are not only quantitatively inaccurate, but more importantly, they are also qualitatively wrong. The one-site model predicts that rapidly moving 3-OMG will accelerate 3-OMG uptake to a greater extent than the slowly moving mannose accelerates mannose entry, when in fact the opposite is found (Table 1).

It is shown that intracellular unstirred layer effects in rat cells do not invalidate the conclusions drawn from the current results. These data are inconsistent with the one-site transporter and are similar to earlier findings [26,27] but without the ambiguities associated with human cells.

Two-site simultaneous transporter. Fitting the observed data for *zero-trans* sugar influx to two-site model parameters is a simpler procedure than with the one-site model. Net flux is defined by a single transport coefficient, k_3 and two affinities at the inside and outside surface. The maximal rate of mannose uptake over 10 min, with 20 mM sugar in the external solution and zero sugar initially present within the cells, is shown as a function of k_3, the inter-site mobility (Fig. 8). A value of k_3 in the range 0.05–1.0 min^{-1} simulates mannose uptake and 3-OMG net uptake is matched by a value of $k_3 = 0.4$–0.45 min^{-1}.

Incorporation of these values of k_3 into a two-site model simulating *infinite-trans* exchange uptakes for mannose and 3-OMG (Fig. 9) shows that the predicted *infinite-trans* V_{max} values for both mannose, (3.0–3.3 μmol(10 min)$^{-1}$(ml cell water)$^{-1}$) and 3-OMG (3.5–4 μmol(10 min)$^{-1}$(ml cell water)$^{-1}$) coincide almost exactly with the observed values for *infinite-trans* V_{max} values mannose/mannose exchange (3.01 ± 0.02 μmol(10 min)$^{-1}$(ml cell water)$^{-1}$) and for 3-OMG/3-OMG exchange (3.46 ± 0.04 μmol(10 min)$^{-1}$(ml cell water)$^{-1}$) (Table 1). The predicted range of two-site model values of *infinite-trans* exchange is much more circumscribed than that predicted by the one-site model (cf., Fig. 6). This reduces any unstirred layer error and

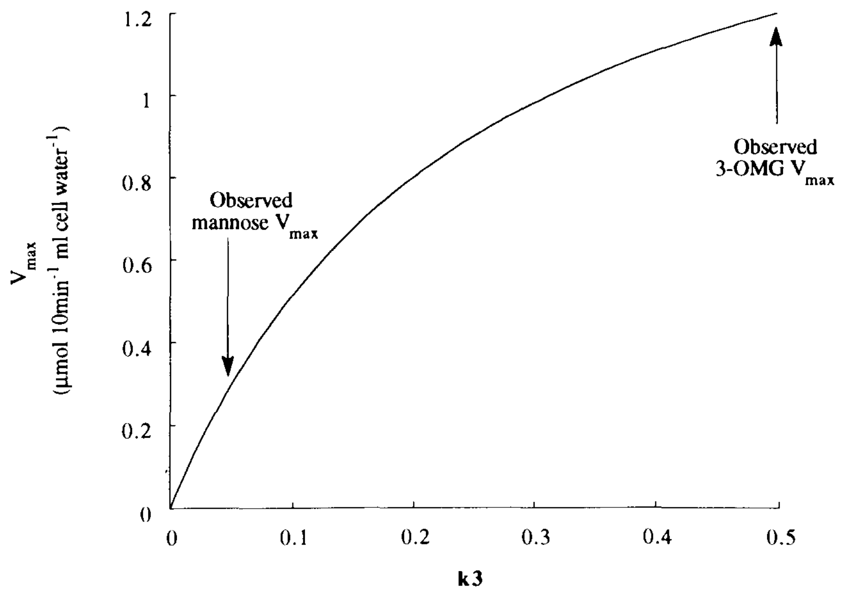

Fig. 8. Simulation from the two-site model of the effects of varying the rate constant, k_3 on the maximal rate of *zero-trans* uptake of 3-OMG and mannose by rat red blood cells. This plot was modelled using the Stella II.2.2.1 (High Performance Systems) package for the Macintosh computer, in order to simulate the initial uptake (10 min) of 3-OMG and mannose by erythrocytes. The observed maximal rates of *zero-trans* uptake (V_{max}) of mannose and 3-OMG are marked by arrows. k_3 = the symmetrical rate constant of sugar, S (see Diagram 2).

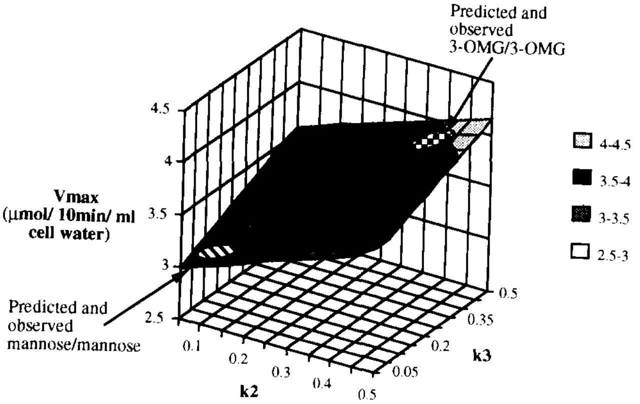

Fig. 9. Contoured surface plot from the two-site model simulating the effects of varying the rate constants k_2 and k_3 on the maximal rate of *infinite-trans* uptake of sugar by rat red cells. This plot shows a simulation from the two-site model of the maximal rate of *infinite-trans* exchange uptake of 3-OMG and mannose over 10 min by rat erythrocytes. The predicted and observed maximal rates (V_{max}) of *infinite-trans* exchange uptake of mannose (striped ellipse) and 3-OMG (chequered ellipse) are superimposed on the surface of the plot. k_2 = the symmetrical rate constant of sugar, R; k_3 = the symmetrical rate constant of sugar, S (see Diagram 2).

the predicted exchange rates increase monotonically with increases in k_2 and k_3.

The contoured surface plot of the two-site model predictions of acceleration ratio with changes in k_2 and k_3 is shown in Fig. 10. The acceleration ratio is maximal when both k_2 and k_3 both have low values. For all values of k_2, (the mobility of the external sugar), raising k_3, (the mobility of the internal ligand), causes a small increase in acceleration ratio; however, as k_2 rises the acceleration ratio reduces. Fig. 10 indicates that mannose should accelerate mannose to a greater extent (8–10-fold) (heavy-striped ellipse) than 3-OMG should accelerate 3-OMG (2.5–3) (heavy-chequered ellipse). This coincides with the observed mannose/mannose acceleration ratio (9.12 ± 0.03) and also with the observed 3-OMG/3-OMG acceleration ratio (2.77 ± 0.14) (Table 1).

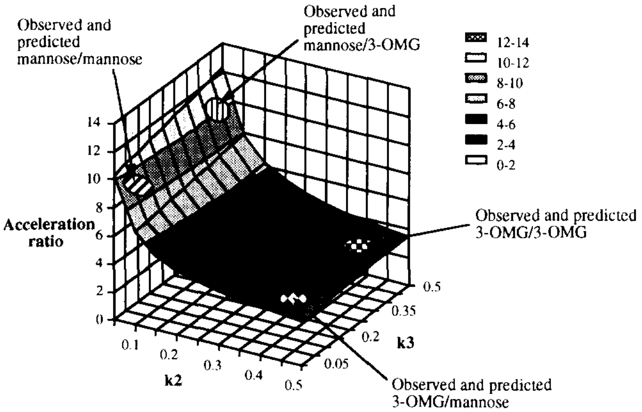

Fig. 10. Contoured surface plot from the two-site model simulating the effects of varying the rate constants k_2 and k_3 on the acceleration ratio of mannose and 3-OMG uptake in rat red cells. The acceleration ratio for sugar uptake is the maximal rate of *infinite-trans* exchange uptake divided by the maximal rate of *zero-trans* uptake. The observed and predicted acceleration ratios for mannose accelerated by mannose (heavy-striped ellipse); mannose accelerated by 3-OMG (light-striped ellipse); 3-OMG accelerated by 3-OMG (heavy-chequered ellipse) and 3-OMG accelerated by mannose (light-chequered ellipse) are superimposed on the surface of the plot. k_2 = the symmetrical rate constant of sugar, R; k_3 = the symmetrical rate constant of sugar, S (see Diagram 2).

The two-site model predictions for hetero-exchange fluxes also match the observed data well. The predicted acceleration ratio of mannose by 3-OMG is 10–12, (light-striped ellipse) and the observed acceleration is 11.76 ± 0.05. This value is significantly greater than the acceleration of mannose by mannose ($P < 0.001$; Table 1). The predicted acceleration ratio of 3-OMG by mannose (2–2.5) is less than the predicted acceleration of 3-OMG by 3-OMG (2.5–3) and similar to the observed ratio (2.12 ± 0.11) (light-chequered ellipse). The observed acceleration ratio of 3-OMG by mannose is significantly less than the observed acceleration ratio of 3-OMG by 3-OMG ($P < 0.001$; Table 1).

The good agreement between the two-site model predictions and the observed data indicate that the two-site model, unlike the one-site mode is consistent with the observed sugar exchange data. The model indicates that sugar flux across the transporter is related to at least two factors. Firstly, to the rate of intersite exchange of doubly liganded sugar, k_{ex}. This is consistent with the the view that accelerated exchange results from a decrease in resistance to intersite flux across the transporter. Secondly, the exchange mobility of sugars appears to correlate with the average net sugar mobility ($k_2 + k_3$), since the exchange rate of the more mobile 3-OMG is retarded by the less mobile mannose and vice versa. The equation for exchange which best fits the data is:

$$k_{ex} + (k_2 + k_3)/5$$

where $k_{ex} = 0.35\ \mathrm{min}^{-1}$ and k_2 and k_3 are as shown in Figs. 9 and 10. This form of exchange is consistent with the view that the exchanging sugars interact directly within the transporter.

A structural model reconciling the one- and two-site models of sugar transport

The transport path via the glucose transporter is considered to be a series of potential hydrogen bonding sites between the substrate and the amino acid residues lining the pathway. A simple model of the processes considered here is four sets of amino acids numbered 1–4, distributed along the pathway from outside to inside. Sets 1 and 4 are considered to have a lower energy than sets 2 and 3 (Diagram 3).

During *zero-trans* net influx, it is envisaged that sugar binds initially to set 1, which triggers H-bond

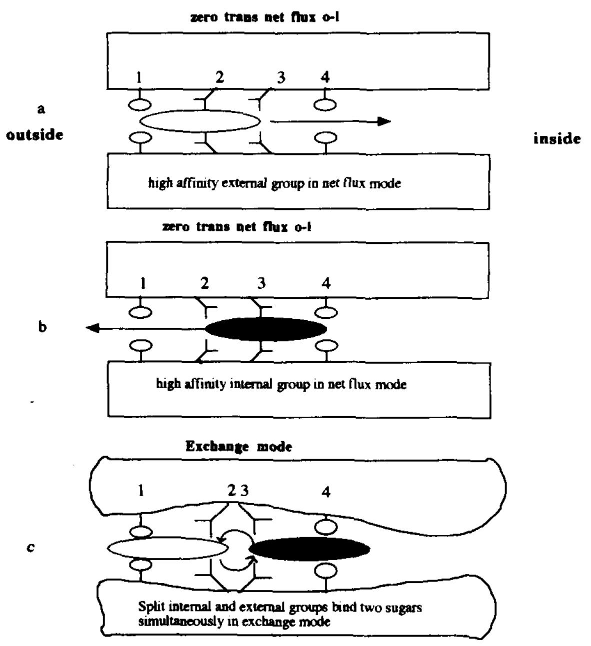

Diagram 3.

alignment in sets 2 and 3 to form additional bonds to the substrate (panel a). Hence, sugar affinity for the transporter increases as the sugar penetrates into the transport pathway. This corresponds with the increase in sugar affinity between K_s and K_m [2,10,28].

Sugar release to the *trans* side may be accompanied by reorientation of the H-bonding groups in sets 2 and 3. *Zero-trans* net efflux follows the reverse pathway (panel b). In this mode the model is a virtual one-site alternating carrier. If sets 1 and 2 differ from sets 3 and 4, the affinities of the transporter for net sugar entry and exit flux pathways may be asymmetric.

Exchange flux here involves simultaneous binding of transported sugars to both sides of the transporter (panel c). External sugar binds to external sites 1 and 2, internal sugar binds to sites 3 and 4. Exchange involves simultaneous transfer of sugars between the alternate sites 1,2 and 3,4. In this mode the transporter behaves as a two-site simultaneous transporter.

In the *net flux* mode each sugar binds to a maximum of 3 sets of ligands; whereas, during the *exchange mode* each of the sugars binds to a maximum of two sets of ligands, this could account for the apparent decrease in affinity and increase in maximal transport rate of the transported sugars during the exchange mode [2].

This structural model also accounts for the apparent one-site binding of non-transported high affinity probes to either the 'internal' or 'external' site on the transporter; i.e., if cytochalasin B binds with high affinity to sets 2–4, maltose, or phloretin binding to sets 1–3 will be prevented, because the H-bonds in set 3 are unfavourably orientated towards internally bound cytochalasin B; similarly, phloretin, or maltose could bind to sets 1–3 and inhibit cytochalasin B binding to sets 2–4 [17–20,29,30].

A similar model has recently been proposed to describe the dual modes of ligand binding in an L-type Ca^{2+} channel [31].

5. Appendix 1

Equations for one-site sequential transport

Diffusion flow of sugars, R and S between found and free cytosolic phases

$$dR/dt = -k_1(\text{bound }[R] - \text{free }[R])$$

$$dS/dt = -k_1(\text{bound }[S] - \text{free }[S])$$

where [R] and [S] are concentrations (mM) of sugars, R and S in the bound and free compartments of the cytosol. Free volume = 1 − (bound volume); bound volume = 0.85.

Membrane flows:

$$dR/dt = -k_3\big(\underbrace{k_2(R_{c_i}\cdot c_o - R_{c_o}\cdot c_i)}_{\text{net flow cycle}} + \underbrace{k_4(Rc_i\cdot S_{c_o} - S_{c_i}\cdot R_{c_o})}_{\text{exchange flow cycle}}\big)$$

$$dS/dt = -k_4\big(\underbrace{k_2(S_{c_i}\cdot c_o - S_{c_o}\cdot c_i)}_{\text{net flow cycle}} + \underbrace{k_3(Sc_i\cdot R_{c_o} - S_{c_o}\cdot R_{c_i})}_{\text{exchange flow cycle}}\big)$$

The constants k_2, k_3 and k_4 are the rate constants of free carrier movement between outside, c_o and inside, c_i and of $R\cdot c_{(o,i)}$ and $S\cdot c_{(o,i)}$ complex movements across the membrane (Diagram 1).

Equilibrium between free sites outside and inside membrane due to site mobility

$$c_i = c_o({}^{re}S_o\cdot k_4 + {}^{re}R_o\cdot k_3 + k_2)/({}^{re}S_i\cdot k_4 + {}^{re}R_i\cdot k_3 + k_2)$$

where ${}^{re}R$ and ${}^{re}S$ are the reduced concentrations of R and S. ${}^{re}R_i$ = free $[R_i]/K_R$; ${}^{re}R_o = R_o/K_R$; ${}^{re}S_i$ = free $[S_i]/K_S$; ${}^{re}S_o = [S_o]/K_S$. $K_R = 1$; $K_S = 1$ and $R_{c_i} = {}^{re}R_i\cdot c_i$; $S_{c_i} = {}^{re}S_i\cdot c_i$; $R_{c_o} = {}^{re}R_o\cdot c_o$ and $S_{c_o} = {}^{re}S_o\cdot c_o$ are the fractional numbers of sites on the inside or outside of the transporter occupied by ligands R and S.

Total free sites outside

$$c_o = T/\big(({}^{re}S_o\cdot k_4 + {}^{re}R_o\cdot k_3 + k_2)/({}^{re}S_i\cdot k_4 + {}^{re}R_i\cdot k_3 + k_2)\cdot(1 + {}^{re}R_i + {}^{re}S_i) + 1 + {}^{re}S_o + {}^{re}R_o\big);\ T = 1$$

6. Appendix 2

Equations for movement of sugars between bound and free cytosolic compartments

$$dR/dt = -k_1(\text{bound [R]} - \text{free [R]})$$

$$dS/dt = -k_1(\text{bound [S]} - \text{free [S]})$$

Bound volume = 0.85; free volume = 1 − (bound volume)

Equations for two-site transmembrane flux of sugars, R and S

$$dR/dt = -k_2\underbrace{\left(x_{R_i}(1 - x_{R_o} - x_{S_o}) - x_{R_o}(1 - x_{R_i} - x_{S_i})\right)}_{\text{net transport } R} - \underbrace{k_{ex2}(x_{R_i} \cdot x_{S_o} - x_{R_o} \cdot x_{S_i})}_{\text{exchange } R}$$

$$dS/dt = -k_2\underbrace{\left(x_{S_i}(1 - x_{S_o} - x_{R_o}) - x_{S_o}(1 - x_{S_i} - x_{R_i})\right)}_{\text{net transport } S} - \underbrace{k_{ex2}(x_{S_i} \cdot x_{R_o} - x_{S_o} \cdot x_{R_i})}_{\text{exchange } S}$$

The exchange transport coefficient was reached by an empirical fit

$$k_{ex2} = (k_{ex} + (k_2 + k_3)/5)$$

where

$$x_{R_i} = {}^{re}R_i/(1 + {}^{re}R_i + {}^{re}S_i)$$

$$x_{R_o} = {}^{re}R_o/(1 + {}^{re}R_o + {}^{re}S_o)$$

$$x_{S_i} = {}^{re}S_i/(1 + {}^{re}R_i + {}^{re}S_i)$$

$$x_{S_o} = {}^{re}S_o/(1 + {}^{re}S_o + {}^{re}R_o)$$

These are the fractional occupancies of R and S ligands on the inside, i and outside, o sites of the transporter (Diagram 2); where, ${}^{re}R_i$ = free $[R_i]/(K_R)$; ${}^{re}R_o = [R_o]/K_R$; ${}^{re}S_i$ = free $[S_i]/(K_S)$ and ${}^{re}S_o = [S_o]/K_S$; as with the one-site transporter (see Appendix 1). $K_R = 1$; $K_S = 1$.

7. References

[1] Wheeler, T.J. and Hinkle, P.C. (1985) Annu. Rev. Physiol. 47, 503-517.
[2] Carruthers, A. (1990) Physiol. Rev. 70, 1135-1176.
[3] Baldwin, S.A. (1992) Biochem. Soc. Trans. 20, 533-537.
[4] Pessin, J.E. and Bell, G.I. (1992) Annu. Rev. Physiol. 54, 911-930.
[5] Thomas, H.M., Brant, A.M., Colville, C.A., Seatter, M.J. and Gould, G.W. (1992) Biochem. Soc. Trans. 20, 538-542.
[6] Baker, G.F. and Naftalin, R.J. (1979) Biochim. Biophys. Acta 550, 474-484.
[7] Weiser, M.B., Razin, M. and Stein, W.D. (1983) Biochim. Biophys. Acta 727, 379-388.
[8] Stein, W.D. (1989) Methods Enzymol. 171, 23-62.
[9] Wheeler, T.J. (1986) Biochim. Biophys. Acta 862, 387-398.
[10] Lowe, A.G. and Walmsley, A.R. (1986) Biochim. Biophys. Acta 857, 146-154.
[11] Wheeler, T.J. and Whelan, J.D. (1988) Biochemistry 27, 1441-1450.
[12] Naftalin, R.J. and Holman, G.D. (1977) in Membrane Transport in Red Cells (Ellory, J.C. and Lew, V.L., eds.), pp. 257-300, Academic Press, London and New York.
[13] Naftalin, R.J., Smith, P.M. and Roselaar, S.E. (1985) Biochim. Biophys. Acta 820, 235-249.
[14] Naftalin, R.J. and Rist, R.J. (1991) Biochim. Biophys. Acta 1064, 37-48.
[15] Helgerson, A.L. and Carruthers, A. (1989) Biochemistry 28, 4580-4594.
[16] Whitesell, R.R., Regen, D.M., Beth, A.H., Pelletier, D.K. and Abumrad, N.A. (1989) Biochemistry 28, 5618-5625.
[17] Deves, R. and Krupka, R.M. (1984) Biochim. Biophys. Acta 769, 455-460.
[18] Krupka, R.M. (1985) J. Membr. Biol. 83, 71-80.
[19] Krupka, R.M. (1989) Biochem. J. 260, 885-891.
[20] Carruthers, A. and Helgerson, A.L. (1991) Biochemistry 30, 3907-3915.
[21] Sogin, D.C. and Hinkle, P.C. (1980) Biochemistry 19, 5417-5420.
[22] Lowe, A.G. and Walmsley, A.R. (1987) Biochim. Biophys. Acta 903, 547-550.
[23] Chin, J.J., Jhun, B.H. and Jung, C.Y. (1992) Biochemistry 31, 1945-1951.
[24] Janoshazi, A. and Solomon, A.K. (1993) J. Membr. Biol. 132, 167-178.
[25] May, J.M. and Beechem, J.M. (1993) Biochemistry 32, 2907-2915.
[26] Miller, D.M. (1968) Biophys. J. 8, 1329-1338.
[27] Naftalin, R.J. (1971) Biochim. Biophys. Acta 233, 635-643.
[28] Naftalin, R.J. (1988) Biochim. Biophys. Acta 946, 431-438.
[29] Baldwin, S.A. and Henderson, P.J.F. (1989) Annu. Rev. Physiol. 51, 459-471.
[30] Holman, G.D. and Ress, W.D. (1987) Biochim. Biophys. Acta 897, 395-405.
[31] Yang, J., Ellinor, P.T., Sather, W.A., Zhang, J.F. and Tsien, R.W. (1993) Nature 366, 158-161.